Article:
Greb, Arthur, Niemi, Kari orcid.org/0000-0001-6134-1974, O'Connell, Deborah orcid.org/0000-0002-1457-9004 et al. (1 more author) (2014) Energy resolved actinometry for simultaneous measurement of atomic oxygen densities and local mean electron energies in radio-frequency driven plasmas. Applied Physics Letters. 234105. ISSN 0003-6951

https://doi.org/10.1063/1.4903931

Energy resolved actinometry for simultaneous measurement of atomic oxygen densities and local mean electron energies in radio-frequency driven plasmas

Arthur Greb, Kari Niemi, Deborah O'Connell, and Timo Gans

Citation: Applied Physics Letters **105**, 234105 (2014); doi: 10.1063/1.4903931
View online: http://dx.doi.org/10.1063/1.4903931
View Table of Contents: http://scitation.aip.org/content/aip/journal/apl/105/23?ver=pdfcov
Published by the AIP Publishing

Energy resolved actinometry for simultaneous measurement of atomic oxygen densities and local mean electron energies in radio-frequency driven plasmas

Arthur Greb,[a] Kari Niemi, Deborah O'Connell, and Timo Gans
York Plasma Institute, Department of Physics, University of York, York YO10 5DD, United Kingdom

(Received 30 October 2014; accepted 25 November 2014; published online 11 December 2014)

A diagnostic method for the simultaneous determination of atomic oxygen densities and mean electron energies is demonstrated for an atmospheric pressure radio-frequency plasma jet. The proposed method is based on phase resolved optical emission measurements of the direct and dissociative electron-impact excitation dynamics of three distinct emission lines, namely, Ar 750.4 nm, O 777.4 nm, and O 844.6 nm. The energy dependence of these lines serves as basis for analysis by taking into account two line ratios. In this frame, the method is highly adaptable with regard to pressure and gas composition. Results are benchmarked against independent numerical simulations and two-photon absorption laser-induced fluorescence experiments. [http://dx.doi.org/10.1063/1.4903931]

Atomic oxygen plays a key role in many plasma technologies as diverse as semi-conductor manufacturing, environmental applications, and plasma medicine.[1] Direct measurements of atomic oxygen densities are challenging, requiring, for example, non-linear laser spectroscopy[2] or synchrotron vacuum ultraviolet absorption spectroscopy.[3] More practical non-intrusive monitoring techniques are highly desirable. Therefore, the concept of qualitative actinometry was originally introduced on the basis of observing atomic oxygen emission intensities for monitoring a silicon etch process.[4]

The "classical" actinometry approach then enabled to quantify reactive species densities by deliberately adding a suitable tracer noble gas and observing the ratio of both the tracer gas emission and the optical emission of the reactive species. The reactive species density can be determined under the assumption that the involved excited states are of similar excitation energy and solely populated through direct electron-impact excitation from the corresponding atomic ground state.[5] The time averaged emission intensity $\langle I \rangle_{rf}$ from one of the states is given by $\langle I \rangle_{rf} = h\nu\, a_{ik} \langle k_e n_e \rangle_{rf}\, n_0$. Here, $h\nu$ denotes the photon energy, k_e is the excitation rate coefficient, n_e is the electron density, n_0 is the ground state density, and a_{ik} is the optical branching ratio. The a_{ik} equates the ratio of the Einstein coefficient for spontaneous emission A_{ik} and the optical decay rate of the excited state A_i, which includes effective collisional quenching.[6,7]

The classical approach can be extended to account for the production of excited atomic oxygen atoms through the dissociative excitation channel. This requires specific knowledge of the electron energy distribution function (EEDF) because both the direct and dissociative excitation processes generally have cross-sections of different shapes and thresholds.[8,9] However, it is not trivial to determine the high energy tail of the EEDF, so that the effective excitation rate coefficients are often either treated as constant or based on simplified assumptions of the electron energy distribution.

For oxygen containing discharges, the validity of the actinometry approach has been shown for various plasma sources through observing the upper oxygen O($3p^3P$) ($\lambda = 844.6$ nm) atomic state and the upper argon Ar($2p_1$) ($\lambda = 750.4$ nm) tracer state.[8,10–14] The atomic oxygen density can then be expressed by

$$n_O = \frac{I_O}{I_{Ar}} \frac{h\nu_{Ar}}{h\nu_O} \frac{k^*_{Ar,d}}{k^*_{O,d}} \frac{a_{ik,Ar}}{a_{ik,O}} n_{Ar} - \frac{k^*_{O,de}}{k^*_{O,d}} n_{O_2}, \tag{1}$$

$$\text{where} \quad k^* = \frac{\langle k_e n_e \rangle_{rf}}{\langle n_e \rangle_{rf}}. \tag{2}$$

The first term of Eq. (1) corresponds formally to the classical actinometry approach and the second term accounts for dissociative excitation. The effective excitation rate coefficient k^* for direct electron-impact excitation is indexed with d, while the dissociative electron-impact excitation is indexed with de. The k^* adequately describes the time and space integrated optical emission intensity, which supports the use of actinometry; however, they generally depend on the electron energy distribution function.

It has already been demonstrated in high pressure micro plasma jets[15] as well as low pressure capacitively coupled plasma discharges[16,17] that this can be overcome by actively coupling measurements with specifically designed numerical simulations.

In this work, a more versatile approach is proposed that does not require an explicit fluid dynamic nor a particle kinetic treatment of the specific plasma. This is achieved by extending the common actinometry approach to also include the atomic oxygen emission from the excited state O($3p^5P$) ($\lambda = 777.4$ nm) and by modifying it to account for the pressure independent excitation ratios instead of the emission intensity ratios. The observation of two excitation ratios instead of one creates a two equation system with two

[a]ag941@york.ac.uk

unknowns and thus opens the possibility to directly measure both the atomic oxygen density and the local mean electron energy simultaneously. The appropriate EEDF is obtained using a simple electron kinetic simulations via the two-term approximation Boltzmann equation solver BOLSIG+.[18] The resulting EEDF space, as a function of mean electron energy, is then used to determine the effective excitation rate coefficients.

To account for the different possible electron-impact excitation channels, here, an effective excitation rate $E^* = \sum_n f_n E^e_{i,n}$ is introduced, which results from the sum over all products of the electron-impact excitation rates $E^e_{i,n}$ and the density fraction f_n of the corresponding collision partner. In case of oxygen, the content of atomic oxygen r_O is defined as the ratio of the atomic and the molecular oxygen densities. The effective excitation ratios as function of the atomic oxygen content r_O and mean electron energy ϵ can then be expressed as

$$\frac{E^*_{844}}{E^*_{750}} = \frac{f_{O_2}}{f_{Ar}} \cdot \frac{r_O\, k_{844,d}(\epsilon) + k_{844,de}(\epsilon)}{k_{750,d}(\epsilon)}, \tag{3}$$

$$\frac{E^*_{777}}{E^*_{750}} = \frac{f_{O_2}}{f_{Ar}} \cdot \frac{r_O\, k_{777,d}(\epsilon) + k_{777,de}(\epsilon)}{k_{750,d}(\epsilon)}. \tag{4}$$

Here, f_{O_2} and f_{Ar} are the oxygen and argon tracer gas fraction, respectively. The advantage of using these ratios is that they are directly accessible from the solution of the two-term Boltzmann equation. These ratios are generally time and space dependent, which complicates the analysis. To overcome this, only the maximum excitation for each considered state is taken into account, since additional excitation processes, such as cascade processes, have the lowest contribution in that case.

Cross section data for direct electron-impact excitation into the $Ar(2p_1)$ state are taken from Ref. 19, as well as for the direct and dissociative electron-impact excitation into the $O(3p^5P)$ and $O(3p^3P)$ states from Refs. 20 and 21.

From the measured absolute intensity $I_i(t, x)$, the excitation is obtained from the following relationship:[22]

$$E_i(t,x) = \frac{1}{n_0}\left(\frac{dn_i(t,x)}{dt} + \frac{1}{\tau_{\text{eff}}} n_i(t,x)\right), \tag{5}$$

$$\text{with} \quad n_i \propto \frac{I_i(t,x)}{A_{ik} h\nu_i}, \tag{6}$$

where $E_i(t, x)$ is the time and space dependent excitation function, n_0 is the ground state density, n_i is the excited state density, τ_{eff} is the effective lifetime of excited state i, A_{ik} is the corresponding Einstein coefficient, and $h\nu_i$ is the energy of the emitted light.

The atomic oxygen density is not modulated within an radio-frequency (RF) cycle; however, the electron energy is strongly modulated so that the obtained energy values are to be regarded carefully because they represent a local value. Numerical simulations of the considered system, using a fluid model,[23] show that the energy during maximum excitation can be significantly higher than the average bulk energy. Hence, using Energy Resolved Actinometry (ERA), the obtained electron energy near the plasma surface boundary sheath is distinctively different from the bulk electron energy and represents a value that can be more relevant for technological applications in which the plasma-sheath and plasma-surface dynamics play a significant role.

The investigated plasma is created using a well studied microscale atmospheric pressure plasma jet (μAPPJ) device with an effective electrode length of 30 mm, and a cross section of $1 \times 1\,\text{mm}^2$.[24] The rf power source (*Coaxial Power Systems RFG*100–13) couples into the μAPPJ via a matching network (*Coaxial Power Systems MMN* 150) at 13.56 MHz. For the phase resolved optical emission spectroscopy measurements, an Intesified Charge-Coupled Device (ICCD) camera (*Andor iStar D334T-series*) with appropriate narrow bandpass filters (*LOT-QuantumDesign:* 750.46 ± 0.50 nm; 777.45 ± 1.75 nm; and 844.79 ± 0.95 nm) for the three investigated optical emission lines is applied.[15,25]

Figure 1 exemplarily shows the experimentally obtained direct electron-impact excitation leading to the emission of the argon $\lambda = 750.4$ nm optical emission line. The value of maximum excitation, marked by a white x, is used equivalently for all three observed lines to obtain the excitation ratios described in Eqs. (3) and (4). Thereby, the determination of atomic oxygen densities and mean electron energies is localized in the spatial and temporal domains.

According to independent experimental observations and simulations[23] for an equivalent μAPPJ device, the dissociation fraction of oxygen is in the range of 2%–4% and the local mean electron energies are about 4.2 eV at the position of maximum excitation. Typically, the μAPPJ is operated with a helium flow of 1 slm (standard liter per minute), an oxygen content of 0.5%, and an argon tracer gas admixture of 0.1%. Figure 2 shows the two simulated effective excitation ratios for values of the dissociation fraction between 0% and 5% over a range of mean electron energies of 3 eV–6 eV for the typical μAPPJ gas composition.

Figure 2(a) shows the effective excitation ratio of the oxygen state $O(3p^3P)$ ($\lambda = 844.6$ nm) and the argon state $Ar(2p_1)$ ($\lambda = 750.4$ nm), and Figure 2(b) shows the excitation ratio of the oxygen state $O(3p^5P)$ ($\lambda = 777.4$ nm) and the

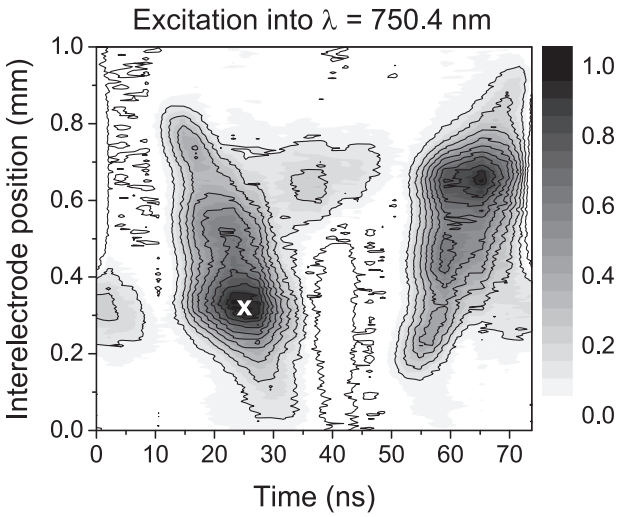

FIG. 1. Excitation leading to the argon optical line emission at $\lambda = 750.4$ nm on a normalized scale. The white x marks the position of maximum excitation, which is used for further analysis.

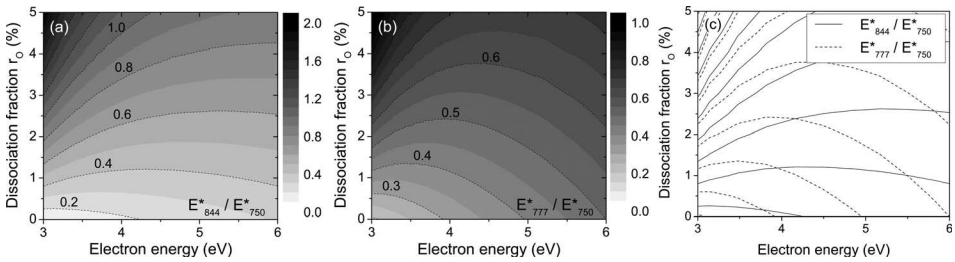

FIG. 2. Simulated effective excitation ratios for (a) E^*_{844}/E^*_{750}, (b) E^*_{777}/E^*_{750}, and (c) overlay of both excitation ratios over a range of dissociation fractions (0%–5%) and mean electron energies (3 eV–6 eV). Gas composition: 99.4% He, 0.5% O_2, and 0.1% Ar; $T_{gas} = 300$ K. Please note that the simulated ratios are significantly influenced by the gas composition.

argon state Ar($2p_1$). For any two given excitation ratios, specific values for the mean electron energy ϵ and dissociation fraction of oxygen r_O can be assigned unambiguously, as shown in Figure 2(c).

Because of the different dependencies of the investigated excitation ratios on electron energies and dissociation fractions, ERA is a sensitive and simple technique, applicable to any pressure regime and highly adaptable regarding the gas composition. However, due to the nature of the actinometry approach, for which emission lines with similar energy thresholds and excitation efficiencies are chosen, the sensitivity for mean electron energy measurements is lower than for the atomic oxygen measurements.

This proposed ERA technique is now demonstrated to quantify local atomic oxygen densities and mean electron energies by observing the ratios at maximum excitation of the argon 750.4 nm, and the oxygen 777.4 nm and 844.6 nm optical emission lines. The obtained results are benchmarked against two-photon absorption laser-induced florescence (TALIF) measurements,[6,26] diagnostic based modeling (DBM),[15,25,27] as well as an extensive fluid model including 116 plasma chemical reactions.[23]

Due to calibration of the optical system, the determined absolute values for the dissociation fraction are subject to an uncertainty of about 6% for elevated power input when the signal-to-noise ratio is high and about 10%–20% when the signal-to-noise ratios drop for lower power inputs. This is reflected in the error bars as shown in Figures 3–5.

From the measured excitation ratios, values for the mean electron energies and atomic oxygen densities under power and oxygen admixture variation can be extracted. The obtained absolute atomic oxygen densities and corresponding dissociation fractions in dependence of the power are shown in Figure 3 using ERA in direct comparison with TALIF, fluid simulations, and DBM. The output of the power supply can be significantly different from the actual plasma power due to losses in the electrical circuit. Therefore, we introduce a normalized power to facilitate the comparison between different experimental setups and numerical simulations. The normalized power is defined as the ratio between the power values P and P_c at which the discharge switches into a spatially constricted high current mode.

Generally, the atomic oxygen densities obtained via TALIF are regarded as the most accurate values. Fluid model simulations overestimate the atomic oxygen density by about a factor of 2.7, while DBM values lie about a factor of 4 above the TALIF measurements. In this respect, our presented ERA diagnostic method is in very good agreement with TALIF measurements and comprises a major improvement over the previous methods.

Regarding an oxygen content variation, TALIF measurements show a maximum of atomic oxygen densities for oxygen admixtures of 0.5%–0.6%.[26] The atomic oxygen density in dependence on the oxygen admixture at constant power (10 W = 0.8 P_c) is shown in Figure 4 in direct comparison with relative [O] density results obtained via nanosecond-TALIF in the plasma core.[26]

The atomic oxygen density increases from about $2.5 \times 10^{21}\,m^{-3}$ at 0.2% oxygen admixture until it reaches a maximum between 0.5% and 0.7% of oxygen admixture. Then, it decreases monotonically towards higher oxygen admixtures due to a decreasing discharge efficiency, since

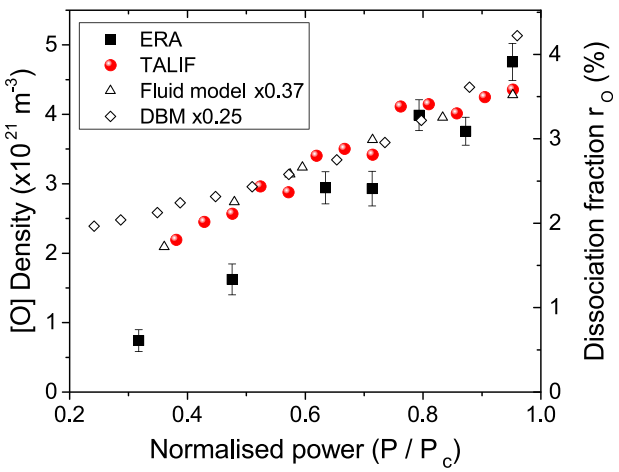

FIG. 3. Atomic oxygen density and dissociation fraction as a function of normalized power (1 slm He, 0.5% O_2, and 0.1% Ar). DBM values are taken from Ref. 15; TALIF and fluid model values are taken from Ref. 23. Reproduced by permission from Waskoenig *et al.*, Plasma Sources Sci. Technol. **19**, 045 018 (2010). Copyright 2010 IOP Publishing.

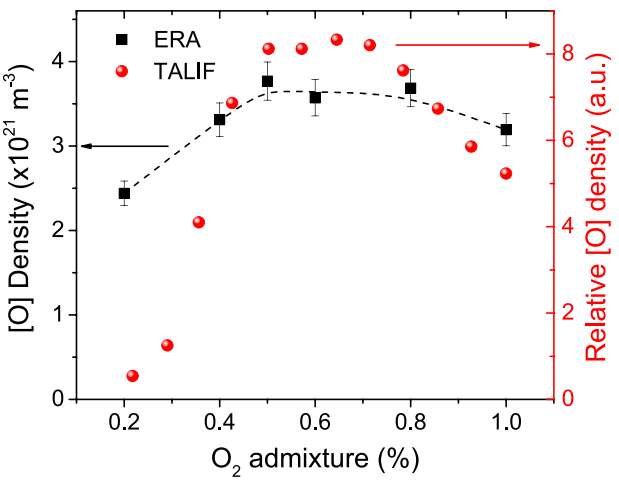

FIG. 4. Atomic oxygen density as a function of O_2 admixture (1 slm He, 0.1% Ar, P = 10 W). TALIF values are taken from Ref. 26.

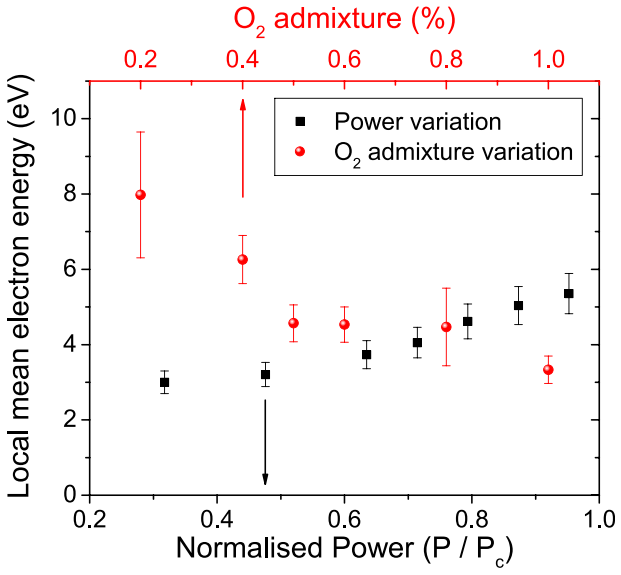

FIG. 5. Local mean electron energy as a function of power (squares, 1 slm He, 0.5% O_2, 0.1% Ar) and O_2 admixture (circles, 1 slm He, 0.1% Ar, P = 10 W).

energy dissipation into molecular states is promoted, finally destabilizing the plasma. The ERA diagnostic technique accurately resembles nanosecond-TALIF measurements and shows even better agreement with our own in-house picosecond-TALIF at the same μAPPJ device.[28]

The local mean electron energies at maximum excitation are shown in Figure 5. With increasing power, the local mean electron energy increases monotonically and is in the range of 3 eV–6 eV, while an increasing oxygen flow leads to a monotonically decreasing local mean electron energy from about 8 eV to 3 eV. In comparison, the bulk energy level lies in the range of 2 eV–3 eV, as shown by numerical simulations.[23]

Concluding, the demonstrated ERA diagnostic technique offers the advantage of being more accurate than classical actinometry and DBM, without the need for full scale and complex plasma kinetic or fluid simulations. Furthermore, expensive laser components as in case of TALIF are not required. By observing the excitation dynamics of three optical emission lines and taking two line ratios, both the atomic oxygen density as well as the local mean electron energy can be determined simultaneously. This can result in a better *in-situ* plasma control and monitoring, where accurate non-intrusive measurements are key, and where it is impractical or impossible to incorporate a laser diagnostic system.

The authors acknowledge Intel Ireland, Ltd. for financial support and the UK Engineering and Physical Sciences Research Council (EPSRC) for supporting this research through the EPSRC Manufacturing Grant No. EP/K018388/1 and the EPSRC Career Acceleration Fellowship (EP/H003797/1).

[1]Plasma 2010 Committee, Plasma Science Committee, and Board on Physics and Astronomy, *Plasma Science: Advancing Knowledge in the National Interest* (The National Academies Press, Washington, DC, 2007).
[2]A. Goehlich, T. Kawetzki, and H. F. Döbele, J. Chem. Phys. **108**, 9362 (1998).
[3]K. Niemi, D. O'Connell, N. de Oliveira, D. Joyeux, L. Nahon, J. P. Booth, and T. Gans, Appl. Phys. Lett. **103**, 034102 (2013).
[4]W. R. Harshbarger, R. A. Porter, T. A. Miller, and P. Norton, Appl. Spectrosc. **31**, 201 (1977).
[5]J. W. Coburn and M. Chen, J. Appl. Phys. **51**, 3134 (1980).
[6]K. Niemi, V. Schulz-von der Gathen, and H. F. Döbele, Plasma Sources Sci. Technol. **14**, 375 (2005).
[7]N. Sadeghi, D. W. Setser, A. Francis, U. Czarnetzki, and H. F. Döbele, J. Chem. Phys. **115**, 3144 (2001).
[8]J. P. Booth, O. Joubert, J. Pelletier, and N. Sadeghi, J. Appl. Phys. **69**, 618 (1991).
[9]M. Adbel-Rahman, V. Schulz-von der Gathen, and T. Gans, Plasma Sources Sci. Technol. **15**, 620 (2006).
[10]H. M. Katsch, A. Tewes, A. Goehlich, T. Kawetzki, E. Quandt, and H. F. Döbele, J. Appl. Phys. **88**, 6232 (2000).
[11]K. J. Taylor and G. R. Tynan, J. Vac. Sci. Technol., A **23**, 643 (2005).
[12]A. Ershov and J. Borysow, Plasma Sources Sci. Technol. **16**, 798 (2007).
[13]R. d'Agostino, F. Cramarossa, S. De Benedictis, and G. Ferraro, J. Appl. Phys. **52**, 1259 (1981).
[14]R. d'Agostino, V. Colaprico, and F. Cramarossa, Plasma Chem. Plasma Process. **1**, 365 (1981).
[15]K. Niemi, S. Reuter, L. M. Graham, J. Waskoenig, and T. Gans, Appl. Phys. Lett. **95**, 151504 (2009).
[16]J. Conway, S. Kechkar, N. O. Connor, C. Gaman, M. M. Turner, and S. Daniels, Plasma Sources Sci. Technol. **22**, 045004 (2013).
[17]A. Greb, K. Niemi, D. O'Connell, and T. Gans, Appl. Phys. Lett. **103**, 244101 (2013).
[18]G. J. M. Hagelaar and L. C. Pitchford, Plasma Sources Sci. Technol. **14**, 722 (2005).
[19]J. E. Chilton, J. B. Boffard, R. S. Schappe, and C. C. Lin, Phys. Rev. A **57**, 267 (1998).
[20]R. R. Laher and F. R. Gilmore, J. Phys. Chem. Ref. Data **19**, 277 (1990).
[21]M. B. Schulman, F. A. Sharpton, S. Chung, C. C. Lin, and L. W. Anderson, Phys. Rev. A **32**, 2100 (1985).
[22]T. Gans, D. O'Connell, V. Schulz-von der Gathen, and J. Waskoenig, Plasma Sources Sci. Technol. **19**, 034010 (2010).
[23]J. Waskoenig, K. Niemi, N. Knake, L. M. Graham, S. Reuter, V. Schulz-von der Gathen, and T. Gans, Plasma Sources Sci. Technol. **19**, 045018 (2010).
[24]V. Schulz-von der Gathen, L. Schaper, N. Knake, S. Reuter, K. Niemi, T. Gans, and J. Winter, J. Phys. D: Appl. Phys. **41**, 194004 (2008).
[25]K. Niemi, S. Reuter, L. M. Graham, J. Waskoenig, N. Knake, V. Schulz-von der Gathen, and T. Gans, J. Phys. D: Appl. Phys. **43**, 124006 (2010).
[26]N. Knake, K. Niemi, S. Reuter, V. Schulz-von der Gathen, and J. Winter, Appl. Phys. Lett. **93**, 131503 (2008).
[27]J. Waskoenig, K. Niemi, N. Knake, L. M. Graham, S. Reuter, V. Schulz-von der Gathen, and T. Gans, Pure Appl. Chem. **82**, 1209 (2010).
[28]J. Bredin *et al.*, "Picosecond-TALIF measurements of atomic oxygen in RF driven atmospheric pressure plasma jets," Appl. Phys. Lett. (submitted).